Mitochondrial dynamics and mitophagy are necessary for proper invasive growth in Rice Blast.

Yanjun Kou[1*#], Yunlong He[2#], Jiehua Qiu[1], Shu Yazhou[1], Fan Yang[2], YiZhen Deng[3], Naweed I. Naqvi[2*]

[1]State Key Laboratory of Rice Biology, China National Rice Research Institute, Hangzhou. China 311400

[2]Temasek Life Sciences Laboratory, and Department of Biological Sciences, 1 Research Link, National University of Singapore, Singapore 117604

[3]Guangdong Province Key Laboratory of Microbial Signals and Disease Control, Integrative Microbiology Research Centre, South China Agricultural University, Guangzhou, China 510642

[#]These authors contributed equally to this work.

*For Correspondence: Yanjun Kou; Email: kouyanjun@caas.cn; Tel. (86)-571-6350-1170 and Naweed I. Naqvi; Email: naweed@tll.org.sg; Phone: (65)-6872-7493

Running head: Mitochondrial dynamics in *Magnaporthe* infection

Key words: Mitochondrial fusion and fission, Rice Blast, mitophagy, *Magnaporthe oryzae*-rice interaction, Atg24, Dnm1, Fzo1

Accession numbers: MoDnm1: XP_003717217.1; MoFzo1: XP_003712754.1; MoAtg24: XP_003716251.1

SUMMARY

Magnaporthe oryzae causes Blast disease, which is one of the most devastating infections in rice and several important cereal crops. *M. oryzae* needs to coordinate gene regulation, morphological changes, nutrient acquisition, and host evasion, in order to invade and proliferate within the plant tissues. Thus far, the molecular mechanisms underlying the regulation of invasive growth *in planta* have remained largely unknown. We identified a precise filamentous-punctate-filamentous cycle in mitochondrial morphology during *Magnaporthe*-Rice interaction. Interestingly, loss of either the mitochondrial fusion (MoFzo1) or fission (MoDnm1) machinery, or inhibition of mitochondrial fission using Mdivi-1 caused significant reduction in *M. oryzae* pathogenicity. Furthermore, exogenous carbon source(s) but not antioxidant treatment delayed such mitochondrial dynamics/transition during invasive growth. Such nutrient-based regulation of organellar dynamics preceded MoAtg24-mediated mitophagy, which was found to be essential for proper biotrophic development and invasive growth *in planta*. We propose that precise mitochondrial dynamics and mitophagy occur during the transition from biotrophy to necrotrophy, and are required for proper induction and establishment of the blast disease in rice.

INTRODUCTION

Mitochondria, the semi-autonomous double-membrane bound organelles, generate most of the adenosine triphosphate (ATP) for diverse cellular functions and are involved in various physiological processes including lipid metabolism, redox signalling, calcium- and iron-homeostasis, and programmed cell death (Zemirli & Morel, 2018, Nunnari & Suomalainen, 2012). Depending on the cellular physiology and environment, mitochondria exhibit a variety of morphologies, ranging from elongated and interconnected networks to small spherical organelles. The mitochondrial shape is dynamic and depends on the balance between two opposing processes, fusion and fission, which occur continuously during the growth cycle (Westermann, 2010). Maintaining the mitochondrial morphology in steady state by the balance of fusion and fission activities is critical for living cells. When this equilibrium is broken, mitochondrial shape and dynamics are disturbed leading to important physiological consequences including increased cellular stress and various diseases (Zemirli & Morel, 2018, Rapaport *et al.*, 1998, Guan *et al.*, 1993, Sesaki & Jensen, 2001, Chang & Doering, 2018, Ma *et al.*, 2009, Mozdy *et al.*, 2000, Delettre *et al.*, 2000, Kijima *et al.*, 2005).

The fusion and fission machineries of mitochondria are well conserved from yeast to mammals. In yeast, mitochondrial fusion mainly depends on the transmembrane GTPase Fzo1, membrane anchored dynamin GTPase Mgm1, and Ugo1, which links the

66 outer and inner membrane fusion machineries (Rapaport et al., 1998, Guan et al., 1993,
67 Sesaki & Jensen, 2001). In yeast, the loss of Fzo1, Mgm1, or Ugo1 leads to numerous
68 small fragmented mitochondria due to a block in fusion and amidst ongoing fission of
69 mitochondria (Rapaport et al., 1998, Guan et al., 1993, Sesaki & Jensen, 2001). The
70 Fis1-Mdv1/Caf4-Dnm1 complex constitutes the major mitochondrial fission pathway in
71 yeast (Mozdy et al., 2000, Griffin *et al.*, 2005). Fis1, a tail-anchored outer membrane
72 protein, functions as a membrane receptor, and Mdv1/Caf4 serves as an adaptor to
73 recruit dynamin-related protein Dnm1 to the fission sites in mitochondria (Mozdy et al.,
74 2000, Griffin et al., 2005). Dnm1 is the key mediator of membrane scission during
75 mitochondrial division (Mozdy et al., 2000). Loss of either Fis1 or Dnm1 blocks fission
76 resulting in highly interconnected fishnet-like mitochondria (Mozdy et al., 2000).
77
78 In addition to fusion and fission machineries, mitochondrial homeostasis requires
79 proper mitophagy, which is the selective sequestration of mitochondria by
80 autophagosomes followed by their degradation in vacuoles/lysosomes (Liu *et al.*, 2014).
81 Mitophagy is a key mechanism in organellar quality control, and is responsible for the
82 removal of damaged or unwanted mitochondria (Liu et al., 2014). In yeast, the
83 mitochondrial outer membrane receptor Atg32 is essential for mitophagy (Kanki *et al.*,
84 2009, Okamoto *et al.*, 2009). In response to nitrogen starvation or inhibition of mTOR
85 following growth in non-fermentable carbon source, Atg32 directs mitochondria to the
86 autophagosome through its interaction with the core autophagic machinery, including
87 Atg8 and Atg11, to induce mitophagy (Kanki et al., 2009, Okamoto et al., 2009). Such

88 receptors sense stimuli that induce mitophagy, and couple mitochondrial dynamics to
89 the quality control machinery (Mao & Klionsky, 2013).
90
91 Although the fusion and fission machineries are highly conserved, diverse
92 mechanisms ensure proper organellar dynamics and distribution to optimize
93 mitochondrial function in response to changing environments and cellular needs. The
94 entire mitochondrial network is fused during G1-S phase transition and
95 fragmented/punctate in the late S and M phase depending on cellular environment in rat
96 kidney cells (Mitra *et al.*, 2009). In addition, the mitochondrial dynamics are modulated
97 in response to certain types and/or severity of stresses and adapt their form by
98 promoting fusion or fission (Shutt & McBride, 2013). When cells are subjected to mild
99 stresses, such as moderate nutrient starvation, protein synthesis inhibition, or mTOR
100 inhibition induced autophagy, mitochondria tend to become more fused to increase ATP
101 production and escape from mitophagy (Tondera *et al.*, 2009, Gomes *et al.*, 2011, Li *et*
102 *al.*, 2015). Conversely, the mitochondrial fission machinery is activated upon prolonged
103 nutrient stress, leading to degradation via mitophagy or apoptosis (Toyama *et al.*, 2016,
104 Frank *et al.*, 2001). It is clear that mitochondrial dynamics and mitophagy are directly
105 associated with metabolic status and stress conditions (Twig *et al.*, 2008, Mao &
106 Klionsky, 2013, Toyama et al., 2016).
107
108 *M. oryzae* is a hemibiotroph, which initially establishes a close biotrophic
109 association to acquire nutrients from the live host cells, but later on switches to the

necrotrophic killing phase to obtain nutrients from dead plant tissues (Fernandez & Orth, 2018). During the infection cycle in *M. oryzae*, the three-celled conidia are deposited by rain splashes and stick to the rice leaf surface. Under proper conditions, such conidia germinate and form appressoria to assist in the breach of the rigid rice cuticle. Once inside the host cell, *M. oryzae* differentiates into invasive hyphae and spreads to neighbouring cells resulting in typical lesion formation. During invasive growth, *M. oryzae* needs to coordinate the nutrient sensing, gene expression regulation, morphological changes, acquiring nutrients from rice cells, and eluding the plant immunity to adapt to the host milieu (Marroquin-Guzman *et al.*, 2017). The molecular mechanisms involved in regulating mitochondrial homeostasis during invasive growth have not been explored in depth. Recent studies have shown that the complex composed of MoDnm1, MoFis1, and MoMdv1 regulates the mitochondrial fission in *M. oryzae* (Zhong *et al.*, 2016). Disruption of *MoDNM1* or *MoFIS1* results in defects in mitochondria fission and pathogenicity (Zhong et al., 2016, Khan *et al.*, 2015). Our recent analyses showed that the sorting nexin MoAtg24 is essential for mitophagy and necessary for proper asexual differentiation (He *et al.*, 2013). However, the regulation and function of mitochondrial dynamics and mitophagy during *M. oryzae* development *in planta* need to be further explored.

In this study, a unique filamentous-punctate-filamentous cycle in mitochondrial morphology and dynamics was observed during the early infectious growth of *M. oryzae*. To uncover the role of this specific cycle and mitophagy, mutants defective in

mitochondrial fusion, fission, and mitophagy were generated via deletion of *MoFZO1*, *MoDNM1*, or *MoATG24* respectively. Characterization of *Modnm1*Δ, *Mofzo1*Δ, and *Moatg24*Δ strains and Mdivi-1-based inhibition of mitochondrial division revealed that mitochondrial fusion and fission machineries and mitophagy are required for maintaining mitochondrial dynamics, and are necessary for proper infection and pathogenesis in *M. oryzae*. We provide evidence that carbon source depletion triggers such specific mitochondrial dynamics during the early infection stage. Overall, our study demonstrates that tightly controlled mitochondrial dynamics and mitophagy are required for proper invasive growth during establishment of the blast disease in rice.

RESULTS

Mitochondrial dynamics during *M. oryzae*-rice interaction

We first examined mitochondrial morphology during *in planta* growth of wild-type (WT) *M. oryzae* using the *Mito-GFP* (as the mitochondrial marker (He et al., 2013, Patkar *et al.*, 2012)) strain. The conidia of the *Mito-GFP* strain were inoculated on sheath from 21 d old susceptible rice seedling (*Oryza sativa* L., cultivar CO39), and incubated in a humid chamber at room temperature. Mitochondrial morphology was examined at the following three time points post inoculation: 30 hpi when the fungus successfully penetrated the rice epidermis, 48 hpi when most of invasive hyphae spread into the neighbouring rice cells and necrotrophy starts to occur, and 72 hpi when necrotrophy/lesion formation could be observed. At 30 hpi, the majority of

153 mitochondria (81.2% ± 1.9%) were in a tubular or filamentous network (Figure 1). In
154 contrast, most mitochondria (83.9% ± 9.9%) were fragmented or punctate at 48 hpi
155 (Figure 1). Interestingly, about half of the mitochondria (50.5% ± 5.9%) appeared to be
156 filamentous or tubular again at 72 hpi (Figure 1). However, such specific and dynamic
157 changes in mitochondrial network were not evident during appressorium formation
158 (Figure S1). Such temporal and dramatic changes in mitochondrial morphology
159 indicated that *M. oryzae* likely faces dynamic environmental or cellular changes that
160 significantly impact mitochondrial form/function during the first 72 h of *in planta*
161 growth.
162
163 **The role of mitochondrial dynamics in invasive growth in *M. oryzae***
164 Mitochondrial dynamics through fusion and fission during invasive growth occurred
165 prior to lesion development, raising the possibility that such organellar dynamics might
166 play an important role in the establishment and spread of the blast disease. To determine
167 the role of such changes in morphology and dynamics of mitochondria during *M. oryzae*
168 infection, we generated mutants defective in mitochondrial fission (*Modnm1*Δ, Figure
169 S2) or inhibited mitochondrial fission using Mdivi-1, or disrupted the mitochondrial
170 fusion (*Mofzo1*Δ, Figure S3) to alter the overall mitochondrial network dynamics, and
171 examined their invasive growth and the pathogenicity.
172
173 *MoDnm1* is known as an important mitochondria fission gene in *M. oryzae* (Zhong
174 *et al*., 2016). In our study, *MoDnm1* was simply used as a marker gene for analyzing the

loss of mitochondrial fission in *M. oryzae*. A gene-deletion mutant of *MoDNM1* was generated in the *Mito-GFP* strain. As previously reported (Zhong *et al*., 2016), the *Modnm1*Δ strain exhibited the characteristic tubular or fishnet-like mitochondrial structures (Figure 2a), suggesting that the *Modnm1*Δ is indeed incapable of mitochondrial fission. To verify the role of mitochondrial fission in fungal pathogenicity, the conidial suspension from WT, *Modnm1*Δ, or *Modnm1*Δ complemented strain was used for blast infection assays on rice seedlings. The *Modnm1*Δ strain showed highly reduced pathogenicity and formed small and highly restricted lesions at 7 dpi (Figure 2b, c). Furthermore, mitochondria in *Modnm1*Δ were tubular or filamentous at 30 hpi, 48 hpi, and 72 hpi, while a majority of mitochondria were fragmented/punctate in the WT at 48 hpi (Figure 3). Since the *Modnm1*Δ strain has pleiotropic defects in *M. oryzae*, we also performed the mitochondrial fission inhibitor treatment to confirm the role of mitochondrial fission during blast infection. Treatment with Mdivi-1, which inhibits mitochondrial fission in *M. oryzae* (Zhong et al., 2016), resulted in extensive tubular mitochondrial structures in *M. oryzae*, and significantly reduced the invasive growth in rice cells (Figure 4). Based on these results, we conclude that mitochondrial fission plays an important role in the invasive growth and lesion formation during Rice Blast.

In *S. cerevisiae,* Fzo1 is the first known mediator of mitochondrial fusion (Rapaport et al., 1998, Fritz *et al.*, 2001). Deletion mutant of the orthologous *MoFZO1* harboured punctate mitochondria (Figure 2a), thus indicating a mitochondrial fusion

defect in this *M. oryzae* mutant. Similar to *Modnm1*Δ, the *Mofzo1*Δ strain formed small and restricted blast lesions on rice plants (Figure 2b). Further microscopic observations showed that more than 90% of appressoria penetrated successfully and about 80% infectious hyphae extended to neighbouring cells in the WT and the complemented strain at 40 dpi, while only 67.5% of appressoria penetrated successfully and 21.6% invasive hyphae spread to surrounding cells in the *Mofzo1*Δ strain (Figure 2c; $P<0.005$). We further analyzed the mitochondrial dynamics during the blast infection process. As shown in Figure 3, the mitochondria in *Mofzo1*Δ were punctate at all the time points tested. These results indicated that mitochondrial fusion within the blast pathogen is required for proper invasive growth and lesion formation.

Taken together, we conclude that the mitochondrial fission and fusion machineries are involved in invasive growth in *M. oryzae*; and mitochondrial dynamics plays a crucial role during *Magnaporthe* pathogenesis.

Carbon source depletion triggers mitochondrial fragmentation

Mitochondrial fragmentation can be triggered by multiple environmental factors such as oxidative stress, and carbon source depletion (Zemirli & Morel, 2018). During host invasion, the fungal pathogen generally encounters the plant defense response, oxidative stress, and metabolic stress. We therefore hypothesized that such host response, oxidative, and/or metabolic stress, triggers the specific mitochondrial fragmentation during invasive growth *in planta*.

To test whether the live host factors trigger such changes in mitochondrial fragmentation, we first examined the mitochondrial morphology in the blast fungus in live host tissue and compared it to that in heat-killed rice sheath. The heat treatment was used to first kill the rice sheath cells before inoculating with the blast fungal strain of interest. Mitochondrial fragmentation was evident in invasive hyphae in heat-killed rice sheath at 48 hpi. However, the percentage of filamentous mitochondria was significantly higher than the control samples at 48 hpi and did not show any difference at 72 hpi (Figure 5). These results indicated that the mitochondrial fragmentation observed during *M. oryzae* invasive growth is dependent in part on the active defense response in addition to other factors in live host plants.

Oxidative stress could trigger the mitochondrial fragmentation in *M. oryzae* (Figure S4). We further tested whether oxidative stress triggers the mitochondrial fragmentation during invasive growth, by imaging the mitochondrial morphology at 30 hpi, 48 hpi, and 72 hpi in the presence of the exogenous antioxidant. The antioxidant treatment was initiated at 24 hpi. In the presence of 2.5 mM GSH (Glutathione) as an exogenous antioxidant, around 81% mitochondria still became punctate or fragmented at 48 hpi (Figure S5). At 72 hpi, filamentous or tubular mitochondria were apparent in GSH-treated invasive hyphae. Likewise, N-acetyl cysteine (NAC) treatment did not alter the mitochondrial fragmentation regime at 48 hpi (Figure S5). Therefore, we

240 inferred that ROS/oxidative stress is unlikely to be the trigger for mitochondrial
241 fragmentation during *M. oryzae* invasive growth.
242
243 Next, we examined the role of carbon source depletion on mitochondrial
244 fragmentation as exogenous carbon sources have been reported to alter metabolic
245 stresses (Toyama et al., 2016). The carbon source, glucose or sucrose, was individually
246 added into inoculated conidia droplets on the rice sheath surface at 24 hpi.
247 Mitochondrial morphology was assessed using a confocal microscope at 30 hpi, 48 hpi,
248 and 72 hpi. We found that excess glucose or sucrose significantly delayed the
249 mitochondrial fragmentation (Figure 6, 7), which indicated that carbon source depletion
250 might be the major factor triggering mitochondrial fragmentation during *in planta*
251 growth in *M. oryzae*. In the control experiments (no additional carbon source), around
252 84% mitochondria appeared fragmented at 48 hpi (Figure 6, 7), whereas mitochondrial
253 fragmentation occurred at 72 hpi in the presence of the indicated exogenous carbon
254 source. At 72 hpi, 69% and 67% of mitochondria were punctate upon additional supply
255 of glucose or sucrose, respectively (Figure 6, 7), while more than 50% mitochondria in
256 the WT appeared filamentous again. Based on these data, we conclude that the presence
257 of excess carbon source impacts mitochondrial dynamics (and/or function) in invasive
258 hyphae during blast development. Since the aforementioned carbon sources delay
259 mitochondrial fragmentation to some extent, it is possible that downstream molecules in
260 the carbon metabolic pathway regulate mitochondrial dynamics during blast infection.
261 Accordingly, the important carbon metabolic intermediate G6P (Glucose-6-phosphate)

was added to the inoculated conidial suspension at 24 hpi, and the mitochondrial morphology was assessed at 48 hpi and 72 hpi. Nearly 85% and 64% of total mitochondria remained tubular or filamentous in the presence of G6P around 48 hpi ($P<0.001$) and 72 hpi (Figure 6, 7; $P<0.01$). Taken together, these results indicate that carbon source depletion and the live host factors but not oxidative stress *per se*, trigger mitochondrial fragmentation during the invasive growth phase in *M. oryzae*.

Mitophagy is necessary for blast infection

As shown in Figure 1, 3, 6, and 8d, the vacuolar localization of Mito-GFP (mitochondrial marker) was observed at 48 hpi and 72 hpi (Figure S6), indicating that mitophagy is likely induced to degrade mitochondria during the initial stages of establishment of the blast disease. Our previous study showed that MoAtg24 is specifically required for mitophagy and is necessary for proper asexual differentiation (He et al., 2013). To determine whether mitophagy plays any role during infection, the pathogenicity of *Moatg24*Δ was tested using rice seedling infection assays. Compared to the WT, which caused the characteristic spindle-shaped blast lesions with grey centres, the *Moatg24*Δ showed highly reduced pathogenicity in rice (Figure 8a). Typical blast disease lesions were not elaborated in the susceptible rice cultivar inoculated with *Moatg24*Δ conidia, while only small lesions were occasionally evident (Figure 8a).

To understand the differences between infection by *Moatg24*Δ and WT conidia, invasive hyphae were observed under the microscope at 30 hpi, 48 hpi, and 72 hpi. At

284 40 hpi, nearly 90% of WT appressoria successfully penetrated the rice sheath. By
285 contrast, less than 20% of *Moatg24*Δ appressoria were capable of invading the rice
286 sheath (Figure 8b; P<0.001). At 48 hpi, although the penetration rates of appressoria in
287 WT and *Moatg24*Δ were comparable, the secondary invasive hyphae were highly
288 reduced in the *Moatg24*Δ (less than 2%) compared to WT (around 80%) (Figure 8b;
289 P<0.001). At 72 hpi, the difference in invasive hyphae in *Moatg24*Δ and WT was more
290 pronounced. The invasive hyphae of WT had successfully spread into 5 to 7 rice cells,
291 whereas the invasive hyphae of *Moatg24*Δ were mainly restricted to the first invaded
292 cells in the rice epidermis (Figure 8c). In rare cases, the invasive hyphae of *Moatg24*Δ
293 could be found within the neighbouring cells surrounding the primary infected rice
294 epidermal cell. Based on these results, we inferred that the highly reduced pathogenicity
295 of *Moatg24*Δ is a result of lack of spread of invasive hyphae from the site of host
296 entry/invasion.
297
298 Since MoAtg24 is essential for mitophagy, and the *Moatg24*Δ showed highly
299 reduced invasive growth in this study, it became important to assess and confirm
300 whether MoAtg24-based mitophagy occurs naturally during blast infection. As shown
301 in Figure 8d, Mito-GFP signal could be detected in vacuoles (CMAC staining), at 60
302 hpi in invasive hyphae (Figure 8d, upper panel). In contrast, such Mito-GFP signal did
303 not colocalize with the vacuoles in invasive hyphae in *Moatg24*Δ (Figure 8d, lower
304 panel), indicating that mitophagy during infection-related growth of *M. oryzae* is
305 blocked in *Moatg24*Δ mutant. Considering that the *Moatg24*Δ mutant is defective in

306 invasive growth and failed to form blast lesions, these results showed that
307 *MoATG24*-mediated mitophagy plays a critical role in the infection process of *M.*
308 *oryzae.*

309

310 Taken together, our data support that mitochondrial dynamics and mitophagy are
311 important intermediate events between nutrient sensing and homeostasis in *M. oryzae*
312 leading to the establishment and extent of the devastating blast disease in rice.

313

314 **DISCUSSION**

315 The adaptation of the mitochondrial fusion and fission to cellular demands is critical for
316 a number of important physiological processes (Zemirli & Morel, 2018). The defects in
317 mitochondrial dynamics cause severe physiological consequences and lead to a variety
318 of dysfunctions (Delettre et al., 2000, Zemirli & Morel, 2018, Kijima et al., 2005), thus
319 highlighting that fusion and fission process must be tightly controlled. In this study, the
320 mitochondrial dynamics were first observed during the early stages of the infection
321 cycle of *M. oryzae*. Interestingly, we uncovered a unique
322 filamentous-punctate-filamentous transition cycle in mitochondrial morphology during
323 *in planta* growth. We demonstrated that the key regulators of mitochondrial fusion and
324 fission are essential for proper mitochondrial dynamics and invasive growth in *M.*
325 *oryzae*. These results suggest that mitochondrial fusion and fission are tightly controlled

326 during blast infection; and that such sequential change in organellar morphology is
327 important for pathogenesis of *M. oryzae*.
328
329 Mitochondrial fragmentation could be triggered by multiple environmental factors
330 or stressors. The blast pathogen generally encounters host defense, oxidative stress, and
331 metabolic stress that may trigger such mitochondrial fragmentation. We propose that
332 carbon source depletion is one of the important factors triggering mitochondrial
333 fragmentation during *in planta* growth of *M. oryzae*. Firstly, mitochondrial
334 fragmentation was observed in the invasive hyphae in heat-killed rice sheath, which is
335 incapable of mounting the defense response. Secondly, exogenous antioxidants did not
336 inhibit or delay such fragmentation processes during infection. Carbon sources (such as
337 glucose or sucrose) or the important metabolic intermediate (G6P) delayed
338 mitochondrial fragmentation, whereas prolonged nutrient starvation induced the
339 breakdown of mitochondrial network in *M. oryzae* (Figure S7). In addition, we found
340 that NH_4NO_3 treatment did not change the mitochondrial morphology (Figure S8),
341 indicating that nitrogen starvation is likely not an important factor that leads to
342 mitochondrial fragmentation during blast infection. Strigolactone is a plant hormone
343 which is associated with mitochondrial biogenesis, fission, fusion, spore germination
344 and hyphal branching in some fungal genera (Besserer *et al.*, 2006). Strigolactone
345 (GR24) treatment did not inhibit the mitochondrial fragmentation processes during
346 *Magnaporthe* infection (Fig S8).
347

348 *M. oryzae* initially acquires nutrients from living host cells, but switches to the
349 necrotrophic killing phase to acquire nutrients from dead tissues between 48 and 72 hpi
350 (Figure S9c). During the transition to necrotrophy, the filamentous invasive hyphae of
351 *M. oryzae* maintain viability as the fungal lifestyle changes and lesion development
352 when host cell death is occurring (Kankanala *et al.*, 2007, Fernandez & Orth, 2018,
353 Jones *et al.*, 2016). *M. oryzae* thus needs to adapt to and overcome nutrient stress prior
354 to switching to the necrotrophic phase. Our results showed that glucose or sucrose
355 supplementation promotes proliferation of invasive hyphae and decreases the cell death
356 in rice during early infection of *M. oryzae* (Figure S9). These results suggest that carbon
357 source depletion occurs during infection and is likely a major factor which triggers the
358 biotrophy-necrotrophy transition. However, carbon starvation and then carbon source
359 acquisition from dead plant tissues may not be the only factor that triggers mitochondria
360 fragmentation and rebuilding of the network, since addition of glucose every 6 h after
361 24 hpi, simply delayed the fragmentation of mitochondria (Figure 6, 7). It is possible
362 that other signals cooperate with carbon homeostasis machinery to regulate and control
363 the mitochondrial morphology/function during the blast infection in rice. In conclusion,
364 our study suggests that carbon source depletion with other factor(s) trigger(s)
365 mitochondrial fragmentation and biotrophic-necrotrophic phase switch during infection
366 of *M. oryzae*.
367
368 In this study, we found that mitophagy is induced along with precise mitochondrial
369 fragmentation during rice blast. Furthermore, mitophagy plays a critical role in invasive

growth of *M. oryzae* in response to energy demands and nutrient homeostasis. It has been suggested that mitophagy requires efficient fission to separate out damaged or unwanted mitochondria to fit into the autophagosomes (Mao & Klionsky, 2013). Thus, it is possible that mitochondrial fragmentation together with ensuing mitophagy is the strategy employed by *M. oryzae* to separate and degrade the damaged/excess mitochondria in order to protect itself in the hostile environment *in planta*.

In conclusion, our study revealed that a unique filamentous-punctate-filamentous cycle in mitochondrial morphology controlled by fission and fusion machinery is important for pathogenesis of *M. oryzae*. Such morphological transitions likely couple with nutrient homeostasis (particularly carbon source) and biotrophy-to-necrotrophy switch during *M. oryzae* infection. In addition, mitophagy regulates the precise turnover of mitochondria, and plays a critical role during the initiation of the devastating blast disease in rice.

EXPERIMENTAL PROCEDURES

Fungal strains and culture media

The *M. oryzae* WT strain B157 (field isolate, *mat1-2*) was a kind gift from the Indian Institute of Rice Research (Hyderabad, India). The *M. oryzae* strains *Mito-GFP*, *Moatg24*Δ, and *Moatg24*Δ-C have been described in our previous reports (Patkar et al., 2012, Ramos-Pamplona & Naqvi, 2006, He et al., 2013).

391

392 *M. oryzae* strains were grown on prune agar (Yeast extract 1 g/L, lactose 2.5 g/L,
393 sucrose 2.5 g/L, prune juice 40 mL/L, agar 20 g/L, pH 6.5) medium at 28℃ in the dark
394 for 2 days, followed by growth under continuous light for 5 days to collect conidia for
395 infection assay. Mutants generated by *Agrobacterium tumefaciens*-mediated
396 transformation (ATMT) were selected on either Complete medium (CM: Casein
397 Hydrolysate 6 g/L, Sucrose 10g/L, Yeast Extract 6 g/L, Agar 20 g/L) containing
398 Hygromycin (250 μg/ml) or Basal medium (BM: Asparagine 2.0 g/L, Yeast Nitrogen
399 Base 1.6 g/L, NH_4NO_3 1.0 g/L, Glucose 10 g/L, Agar 20g/L, pH 6.0) with
400 Chlorimuron-ethyl (50 μg/ml) or with Ammonium glufosinate (50 μg/ml).

401

402 **Construction of *Modnm1*Δ and *Mofzo1*Δ strains and complementation analyses**

403 The *MoDNM1* gene (*MGG_06361*) deletion mutant was generated using the standard
404 one-step gene replacement strategy. Briefly, about 1 kb (kilobase) of 5' UTR and 3'
405 UTR regions were PCR amplified and ligated sequentially to flank the $ILV2^{SUR}$
406 sulfonylurea-resistance cassette in pFGL820 (Addgene, 58221) (Figure S2a). The
407 following primers were used to amplify the 5' and 3' UTR of the *MoDNM1* gene:
408 Dnm1-5F (5'-GAGAGTGTT GAATTC CTCACGGGATGGGCTTCTG-3') Dnm1-5R
409 (5'-GAGAGTGTT GGTACC GGCGAAAATCGGTTCCGTGGTC-3'), Dnm13-F
410 (5'-GAGAGTGTT GTCGAC TGAAGCTGTTTGCGCCATG-3'), and Dnm13-R
411 (5'-GAGAGTGTT GCATGC TACCTATGATCAGCCCGC-3'). Underlined sequences
412 are restriction sites introduced for cloning purpose. The final plasmid construct was

413 confirmed by sequencing and subsequently introduced into the *Mito-GFP* strain by
414 ATMT to replace the *MoDNM1* gene (Yang & Naqvi, 2014). All the correct
415 transformants in this study were ascertained by locus-specific PCR and/or Southern blot
416 analysis (Figure S2b, S3b). For complementation analysis, the full length genomic copy
417 with promoter of *MoDNM1* was amplified with MoDnm1-F (5'-AATT GAATTC
418 GTTGAGCAGGCCGAGCGAC-3') and MoDnm1-R (5'-AATT GAATTC
419 CACTGGCATTTGATTACGCAAGG-3') inserted into pFGL822 (Addgene, 558226)
420 and introduced into the *Modnm1*Δ strain.
421
422 For generating the plasmid vector for *MoFZO1* (*MGG_05209*) deletion, about 1 kb
423 of 5' UTR and 3' UTR regions were PCR amplified and ligated sequentially to flank the
424 *phosphinothricin acetyl transferase* gene cassette in pFGL822 (Figure S3). The
425 following primers were used to amplify the 5' and 3' UTR of the Mo*Fzo1* gene: Fzo1-5F
426 (5'-GAGAGTGTT GAATTC ACTCGGCCGCGATACGCTGC-3'), Fzo1-5r
427 (5'-GAGAGTGTT GGATCC GTGATCGATTTCGTCCAGTC-3'), Fzo1-3F
428 (5'-GAGAGTGTT CTGCAG GCAGAACCATCCTCGTCGTC-3'), and Fzo1-3r
429 (5'-GAGAGTGTT AAGCTT CCTGGCGGCGGCGACATCAAC-3'). The final
430 plasmid was introduced into the *Mito-GFP* strain by ATMT to replace the *MoFZO1*
431 gene. The complementation fragment, which contains the full length genomic copy with
432 promoter of *MoFZO1* gene, was amplified with MoFzo1-F (5'-AATT GGATCC
433 GGCTGTCTGCGTGATCCCTG-3') and MoFzo1-R (5'-AATT TCTAGA

GCTGTGGAGCGAGGAGCAGG-3') and inserted into pFGL899 to complement the *Mofzo1*Δ strain (Yang & Naqvi, 2014).

Infection assays

For blast infection assay, conidial suspension (10^6/mL) with 0.01% gelatine was sprayed on 21 day old rice seedlings (*Oryza sativa* L., cultivar CO39) and incubated in a growth chamber (16 h light/d, 22℃ and 90% humidity). Blast disease in infection assays were assessed and recorded by scanning the leaves at 7 days post inoculation. The blast infection assays were repeated at least three times.

For the host penetration and *in planta* invasive hyphal development assay, healthy rice seedlings (CO39) at the age of 4 weeks were selected for sheath preparation. Conidial suspension ($5x10^4$/ mL) were inoculated onto rice sheath and incubated on the sterile wet tissue paper in the 90 mm Petri dish. Then the petri dishes with inoculated rice sheaths were transferred into the growth chamber with a photoperiod of 16 h: 8 h light: dark cycle at 25℃. The inoculated sheath was trimmed manually and observed by using an Olympus BX51 wide field microscope or with a laser scanning confocal microscope at selected time points.

To prepare heat-killed rice sheaths, the fresh rice sheaths were immersed into sterile water at 70℃ for 25 min (Shipman *et al.*, 2017). The heat-killed rice sheath has

455 the physical structures of cells, while the abilities of host response to fungal infection
456 are lost.
457
458 **Carbon sources, antioxidant, and Mdivi-1 treatments**
459 For treatments with excess carbon sources, the conidia from the tested strains were
460 inoculated on to rice sheath and incubated in growth chamber. At 24 hpi (hours post
461 inoculation), the water on the rice sheath was removed, and then following solutions
462 were applied to the sheath: 8 mg/mL sucrose, 50 mg/mL glucose, 1.5 mg/mL G6P
463 (Glucose-6-phosphate, Sigma-Aldrich), 2.5 mM GSH (L-Glutathione reduced,
464 Sigma-Aldrich), 40 mM NAC (N-acetyl cysteine, Sigma-Aldrich), or 10 mM Mdivi-1
465 (Selleck). The rice sheaths were incubated in the growth chamber until observation.
466 These experiments were repeated thrice.
467
468 **Vacuolar staining**
469 The infected rice sheaths were incubated with CellTracker™ Blue CMAC Dye
470 (7-amino-4-chloromethylcoumarin, Molecular Probes, C2110) at a final working
471 concentration of 10 μM for 2 h at 37 °C. The sample was washed with water prior to
472 microscopic observation.
473
474 **Live cell imaging and image processing**
475 Live cell epifluorescence microscopy was performed with a Zeiss LSM 700 inverted
476 confocal microscope (Carl Zeiss, Inc) using a Plan-Apochromat 63 (NA=1.40) Oil

477 immersion lens. EGFP (Enhanced GFP) and CMAC excitation were performed at 488
478 nm (Em. 505-530 nm) and 405 nm (Em. 430-470 nm) respectively. For *in planta*
479 invasive hyphal development observation, z-stack that consisted of 0.5 μm-space
480 sections was captured for each appressorium penetration site. Image processing was
481 processed in Image J program which was downloaded from National Institutes of
482 Health (http://rsb.info.nih.gov/). The maximum projection of z-stack was obtained by Z
483 projection with max intensity in Image J. 3-D reconstruction, visualization, and analysis
484 were performed in Bitplan Imaris with filament and spots program (Zurich,
485 Switzerland). For figure preparation, the images were arranged in Adobe Illustrator
486 CS6.
487

488 **CONFLICT OF INTEREST**

489 There is no conflict of interest.
490

491 **ACKNOWLEDGEMENTS**

492 We thank the Fungal Pathobiology group at TLL for useful discussion and suggestions.
493 We thank Gu Keyu and Amit Anand for image analyses. This study was supported by
494 the Chinese Academy of Agricultural Sciences under “Elite Youth” program and
495 Agricultural Sciences and Technologies Innovation Program, and the Zhejiang
496 Provincial Natural Science Foundation of China (LQ19C140004). National Research
497 Foundation, Singapore (Prime Minister’s Office, NRF-CRP7-2010-02), and intramural
498 grants from the Temasek Life Sciences Laboratory, Singapore.

Naweed I. Naqvi, Yanjun Kou, and Yunlong He planned and designed the research. Yanjun Kou, Yunlong He, Yazhou Shu, Jiehua Qiu, Fan Yang, and Yizhen Deng performed experiments, conducted fieldwork, analysed data etc. Yanjun Kou, Yunlong He, and Naweed I. Naqvi wrote the manuscript. Yanjun Kou and He Yunlong contributed equally.

REFERENCE

Besserer, A., Puech-Pages, V., Kiefer, P., Gomez-Roldan, V., Jauneau, A., Roy, S., *et al.* (2006) Strigolactones stimulate arbuscular mycorrhizal fungi by activating mitochondria. *PLoS biology*, **4,** e226.

Chang, A. L. and Doering, T. L. (2018) Maintenance of Mitochondrial Morphology in *Cryptococcus neoformans* Is Critical for Stress Resistance and Virulence. **9**.

Delettre, C., Lenaers, G., Griffoin, J. M., Gigarel, N., Lorenzo, C., Belenguer, P., *et al.* (2000) Nuclear gene *OPA1*, encoding a mitochondrial dynamin-related protein, is mutated in dominant optic atrophy. *Nature genetics*, **26,** 207-210.

Fernandez, J. and Orth, K. (2018) Rise of a Cereal Killer: The Biology of *Magnaporthe oryzae* Biotrophic Growth. *Trends in microbiology*, **26,** 582-597.

Frank, S., Gaume, B., Bergmann-Leitner, E. S., Leitner, W. W., Robert, E. G., Catez, F., *et al.* (2001) The role of dynamin-related protein 1, a mediator of mitochondrial fission, in apoptosis. *Developmental cell*, **1,** 515-525.

520 Fritz, S., Rapaport, D., Klanner, E., Neupert, W. and Westermann, B. (2001)
521 Connection of the mitochondrial outer and inner membranes by Fzo1 is critical
522 for organellar fusion. *The Journal of cell biology*, **152,** 683-692.
523 Gomes, L. C., Di Benedetto, G. and Scorrano, L. (2011) During autophagy
524 mitochondria elongate, are spared from degradation and sustain cell viability.
525 *Nature cell biology*, **13,** 589-598.
526 Griffin, E. E., Graumann, J. and Chan, D. C. (2005) The WD40 protein Caf4p is a
527 component of the mitochondrial fission machinery and recruits Dnm1p to
528 mitochondria. *The Journal of cell biology*, **170,** 237-248.
529 Guan, K., Farh, L., Marshall, T. K. and Deschenes, R. J. (1993) Normal mitochondrial
530 structure and genome maintenance in yeast requires the dynamin-like product of
531 the *MGM1* gene. *Current genetics*, **24,** 141-148.
532 He, Y., Deng, Y. Z. and Naqvi, N. I. (2013) Atg24-assisted mitophagy in the foot cells
533 is necessary for proper asexual differentiation in *Magnaporthe oryzae*.
534 *Autophagy*, **9,** 1818-1827.
535 Jones, K., Kim, D. W., Park, J. S. and Khang, C. H. (2016) Live-cell fluorescence
536 imaging to investigate the dynamics of plant cell death during infection by the
537 rice blast fungus *Magnaporthe oryzae*. *BMC plant biology*, **16,** 69.
538 Kankanala, P., Czymmek, K. and Valent, B. (2007) Roles for rice membrane dynamics
539 and plasmodesmata during biotrophic invasion by the blast fungus. *The Plant*
540 *cell*, **19,** 706-724.

Kanki, T., Wang, K., Cao, Y., Baba, M. and Klionsky, D. J. (2009) Atg32 is a mitochondrial protein that confers selectivity during mitophagy. *Developmental cell,* **17,** 98-109.

Khan, I. A., Ning, G., Liu, X., Feng, X., Lin, F. and Lu, J. (2015) Mitochondrial fission protein MoFis1 mediates conidiation and is required for full virulence of the rice blast fungus *Magnaporthe oryzae*. *Microbiological research,* **178,** 51-58.

Kijima, K., Numakura, C., Izumino, H., Umetsu, K., Nezu, A., Shiiki, T., *et al.* (2005) Mitochondrial GTPase *mitofusin 2* mutation in Charcot-Marie-Tooth neuropathy type 2A. *Human genetics,* **116,** 23-27.

Li, J., Wang, Y., Wang, Y., Wen, X., Ma, X. N., Chen, W., *et al.* (2015) Pharmacological activation of AMPK prevents Drp1-mediated mitochondrial fission and alleviates endoplasmic reticulum stress-associated endothelial dysfunction. *Journal of molecular and cellular cardiology,* **86,** 62-74.

Liu, L., Sakakibara, K., Chen, Q. and Okamoto, K. (2014) Receptor-mediated mitophagy in yeast and mammalian systems. *Cell research,* **24,** 787-795.

Ma, H., Hagen, F., Stekel, D. J., Johnston, S. A., Sionov, E., Falk, R., *et al.* (2009) The fatal fungal outbreak on Vancouver Island is characterized by enhanced intracellular parasitism driven by mitochondrial regulation. *Proceedings of the National Academy of Sciences of the United States of America,* **106,** 12980-12985.

Mao, K. and Klionsky, D. J. (2013) Mitochondrial fission facilitates mitophagy in *Saccharomyces cerevisiae*. *Autophagy,* **9,** 1900-1901.

563 Marroquin-Guzman, M., Hartline, D., Wright, J. D., Elowsky, C. and Bourret, T. J.
564 (2017) The *Magnaporthe oryzae* nitrooxidative stress response suppresses rice
565 innate immunity during blast disease. *Nature microbiology,* **2,** 17054.
566 Mitra, K., Wunder, C., Roysam, B., Lin, G. and Lippincott-Schwartz, J. (2009) A
567 hyperfused mitochondrial state achieved at G1-S regulates cyclin E buildup and
568 entry into S phase. *Proceedings of the National Academy of Sciences of the*
569 *United States of America,* **106,** 11960-11965.
570 Mozdy, A. D., McCaffery, J. M. and Shaw, J. M. (2000) Dnm1p GTPase-mediated
571 mitochondrial fission is a multi-step process requiring the novel integral
572 membrane component Fis1p. *The Journal of cell biology,* **151,** 367-380.
573 Nunnari, J. and Suomalainen, A. (2012) Mitochondria: in sickness and in health. *Cell,*
574 **148,** 1145-1159.
575 Okamoto, K., Kondo-Okamoto, N. and Ohsumi, Y. (2009) Mitochondria-anchored
576 receptor Atg32 mediates degradation of mitochondria via selective autophagy.
577 *Developmental cell,* **17,** 87-97.
578 Patkar, R. N., Ramos-Pamplona, M., Gupta, A. P., Fan, Y. and Naqvi, N. I. (2012)
579 Mitochondrial beta-oxidation regulates organellar integrity and is necessary for
580 conidial germination and invasive growth in *Magnaporthe oryzae*. *Molecular*
581 *microbiology,* **86,** 1345-1363.
582 Ramos-Pamplona, M. and Naqvi, N. I. (2006) Host invasion during rice-blast disease
583 requires carnitine-dependent transport of peroxisomal acetyl-CoA. *Molecular*
584 *microbiology,* **61,** 61-75.

585 Rapaport, D., Brunner, M., Neupert, W. and Westermann, B. (1998) Fzo1p is a
586 mitochondrial outer membrane protein essential for the biogenesis of functional
587 mitochondria in *Saccharomyces cerevisiae*. *The Journal of biological chemistry,*
588 **273,** 20150-20155.
589 Sesaki, H. and Jensen, R. E. (2001) *UGO1* encodes an outer membrane protein required
590 for mitochondrial fusion. *The Journal of cell biology,* **152,** 1123-1134.
591 Shipman, E. N., Jones, K., Jenkinson, C. B., Kim, D. W., Zhu, J. and Khang, C. H.
592 (2017) Nuclear and structural dynamics during the establishment of a
593 specialized effector-secreting cell by *Magnaporthe oryzae* in living rice cells.
594 *BMC cell biology,* **18,** 11.
595 Shutt, T. E. and McBride, H. M. (2013) Staying cool in difficult times: mitochondrial
596 dynamics, quality control and the stress response. *Biochimica et biophysica acta,*
597 **1833,** 417-424.
598 Tondera, D., Grandemange, S., Jourdain, A., Karbowski, M., Mattenberger, Y., Herzig,
599 S., *et al.* (2009) *SLP-2* is required for stress-induced mitochondrial hyperfusion.
600 *The EMBO journal,* **28,** 1589-1600.
601 Toyama, E. Q., Herzig, S., Courchet, J., Lewis, T. L., Jr., Loson, O. C., Hellberg, K., *et*
602 *al.* (2016) Metabolism. AMP-activated protein kinase mediates mitochondrial
603 fission in response to energy stress. *Science (New York, N.Y.),* **351,** 275-281.
604 Twig, G., Elorza, A., Molina, A. J., Mohamed, H., Wikstrom, J. D., Walzer, G., *et al.*
605 (2008) Fission and selective fusion govern mitochondrial segregation and
606 elimination by autophagy. *The EMBO journal,* **27,** 433-446.

607 Westermann, B. (2010) Mitochondrial fusion and fission in cell life and death. *Nature*
608 *reviews. Molecular cell biology*, **11,** 872-884.
609 Yang, F. and Naqvi, N. I. (2014) Sulfonylurea resistance reconstitution as a novel
610 strategy for *ILV2*-specific integration in *Magnaporthe oryzae*. *Fungal genetics*
611 *and biology : FG & B*, **68,** 71-76.
612 Zemirli, N. and Morel, E. (2018) Mitochondrial Dynamics in Basal and Stressful
613 Conditions. *International journal of molecular sciences*, **19,** pii: E564.
614 Zhong, K., Li, X., Le, X., Kong, X., Zhang, H., Zheng, X., *et al.* (2016) MoDnm1
615 Dynamin Mediating Peroxisomal and Mitochondrial Fission in Complex with
616 MoFis1 and MoMdv1 Is Important for Development of Functional
617 Appressorium in *Magnaporthe oryzae*. *PLoS pathogens*, **12,** e1005823.

618

619

620 **SUPPORTING INFORMATION LEGENDS**

621 **Figure S1** Mitochondrial morphology during appressorium formation in *M. oryzae*.

622

623 **Figure S2** Generation and verification of *Modnm1*Δ mutant.

624

625 **Figure S3** Generation and verification of *Mofzo1*Δ mutant.

626

627 **Figure S4** Oxidant treatment induces mitochondrial fragmentation.

628

629 **Figure S5** Antioxidant treatment does not delay mitochondrial dynamics during
630 invasive growth.

631

632 **Figure S6** The vacuolar localization of Mito-GFP (mitochondrial marker) during
633 invasive growth.

634

635 **Figure S7** Prolonged nutrient starvation induces mitochondrial fragmentation and
636 mitophagy.

637

638 **Figure S8** NH_4NO_3 or GR24 treatment did not change the mitochondrial fragmentation
639 during infection by *M. oryzae*.

640

641 **Figure S9** Addition of glucose or sucrose promotes spread of invasive hyphae and
642 decreases the cell death in rice during early infection by *M. oryzae*.

643

644

645

646

647

648

649

650 **FIGURE LEGENDS**

651 **Figure 1** Specific changes in mitochondrial morphology during *in planta* growth of *M.*
652 *oryzae*. (a) Mitochondrial morphology in *M. oryzae* during infection. The conidial
653 suspension of the *Mito-GFP* strain was inoculated on rice sheath (*Oryza sativa* L.,
654 cultivar CO39). Confocal microscopy was carried at 30, 48, and 72 hpi. The 3D
655 reconstruction of the mitochondrial morphology was performed in Bitplan Imaris. Red
656 spots and green filaments represent punctate and filamentous mitochondria respectively.
657 Scale bar: 8 μm. (b) Quantification of the different morphologies of mitochondria in the
658 wild type *Mito-GFP* strain during infection. Error bars represent Mean ± SD from three
659 independent replicates. Sample size is more than 200 appressoria penetration sites/host
660 tissue per analysis.

661

662 **Figure 2** Mitochondrial fusion and fission are required for proper pathogenesis of *M.*
663 *oryzae*. (a) The function of *MoDNM1* and *MoFZO1* in mitochondrial fission and fusion.
664 Two day old liquid CM-grown mycelia of the indicated strains were used for imaging
665 with confocal microscopy. Most of the mitochondria in *Modnm1*Δ formed elongated or
666 interconnected fishnet-like structures, while the mitochondria were punctate or
667 fragmented in *Mofzo1*Δ in vegetative mycelia. (b) The rice seedling (*Oryza sativa* L.,
668 cultivar CO39) infection assay of wild type (WT), *Modnm1*Δ, *Modnm1*Δ
669 complementation strain (*Modnm1*Δ-C), *Mofzo1*Δ, and *Mofzo1*Δ complemented strain
670 (*Mofzo1*Δ-C). (c) Detailed observation and statistical analysis of invasive growth in rice
671 sheath cells at 40 hpi. Four types (illustrated in the right panel with corresponding

672 colour labels): no penetration, penetration with primary hyphae, with differentiated
673 secondary invasive hyphae, and invasive hyphae spreading into neighbouring cells,
674 were quantified. Data represent mean ± SD of three independent experiments, with n =
675 200 appressoria per analysis. Scale bar represents 5 μm.
676
677 **Figure 3** The mitochondrial morphology in WT, *Modnm1*Δ, and *Mofzo1*Δ during the
678 infection process. Invasive hyphal growth of *Modnm1*Δ or *Mofzo1*Δ was significantly
679 slower than WT. Scale bar = 10 μm.
680
681 **Figure 4** Chemical inhibition of mitochondrial fission reduces invasive hyphal growth
682 of *M. oryzae*. (a) The mitochondria were predominantly tubular or filamentous upon
683 Midvi-1 treatment. Scale bar represents 2 μm. (b) The mitochondrial morphology of the
684 *Mito-GFP* strain with/without Midvi-1 at 48 hpi. Scale bar = 8 μm. (c) Detailed
685 observation and statistical analysis of invasive growth in rice sheath cells at 48 hpi.
686
687 **Figure 5** The mitochondrial morphology and dynamics in the *Mito-GFP* strain in
688 heat-killed rice sheath. (a) Confocal microscopy images of the *Mito-GFP* strain in dead
689 rice sheath cells at 30, 48, and 72 hpi. Scale bar = 12 μm. In the 3D image, red spots and
690 green filaments highlight punctate and filamentous mitochondria respectively. (b)
691 Quantitative analysis of mitochondria of different morphologies in the *Mito-GFP* strain
692 in heat-killed rice cells. Values represent the mean ± SD from three independent

693 experiments. Sample size is more than 200 appressoria penetration sites per analysis. **,
694 P<0.005 compared with WT at indicated time point.
695
696 **Figure 6** Carbon-replete condition delays mitochondrial fragmentation *in planta*.
697 Conidia of the *Mito-GFP* strain were inoculated onto the rice sheaths. At 24 hpi the
698 fluid in the conidial suspension was replaced with either sterile H_2O (Control), 8 mg/mL
699 sucrose, 50 mg/mL glucose, or 1.5 mg/mL G6P (Glucose-6-phosphate). Confocal
700 microscopy was carried out at 30, 48, and 72 hpi. The right panels show enlarged view
701 of the boxed region in the left panel. Scale bar equals 5 μm.
702
703 **Figure 7** Mitochondrial morphology with or without exogenous sucrose, glucose, or
704 G6P. Values represent the mean ± SD from three independent experiments. ***,
705 P<0.001; **, P<0.005; *, P<0.01 in comparison to control (H_2O) at the same time
706 points. Sample size is more than 200 appressoria penetration sites per analysis.
707
708 **Figure 8** MoAtg24-mediated mitophagy is necessary for *M. oryzae* infection. (a) Loss
709 of *MoATG24* gene leads to reduction in pathogenicity. Blast infection assays of wild
710 type (WT), *Moatg24*Δ, or *Moatg24*Δ complementation strain (*Moatg24*Δ-C) were
711 performed using rice seedlings (*Oryza sativa* L., cultivar CO39). Images were taken at 7
712 dpi. (b) Developmental defects in the invasive hyphae of *Moatg24*Δ strain. The invasive
713 hyphae in rice sheath cells were quantified as descripted in Figure 2c. Data represents
714 the mean ± SD from three independent experiments. More than 200 appressoria from

each indicated strain were assessed each time. (c) Invasive hyphal growth in WT and *Moatg24*Δ strains at 30, 48, and 72 hpi. Scale bar = 12 μm. (d) MoAtg24 is required for mitophagy during *M. oryzae* infection. WT or *Moatg24*Δ strain expressing *Mito-GFP* was inoculated into rice sheaths for 60 h. The vacuoles in invasive hyphae were visualized by staining with CMAC. Scale bar = 2.5 μm.

Figure 1

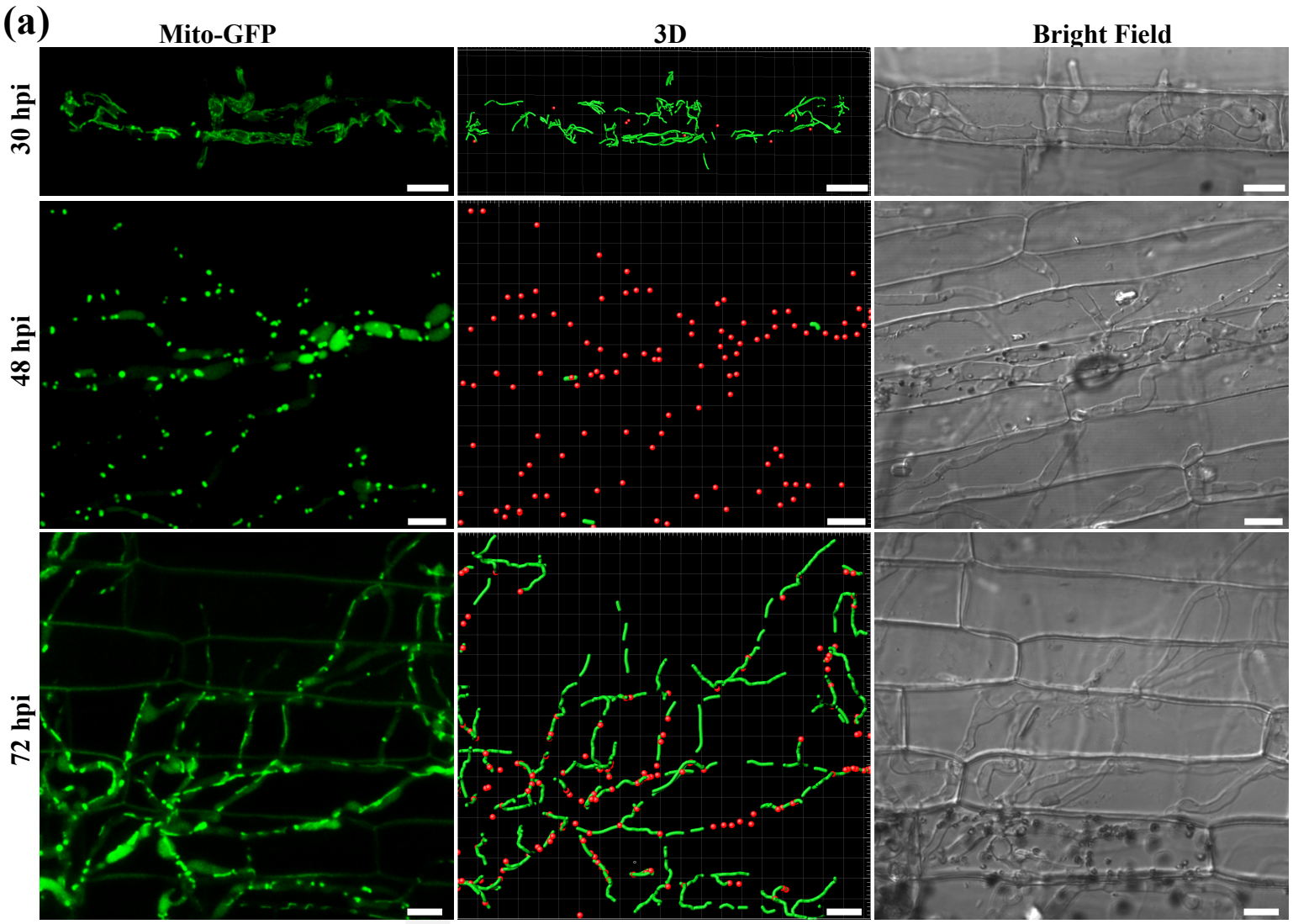

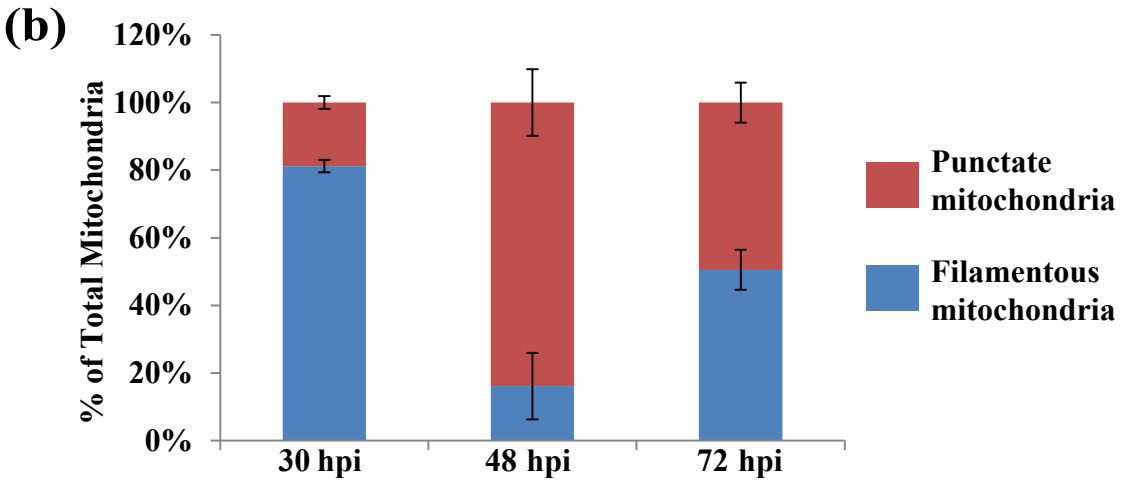

Figure 2

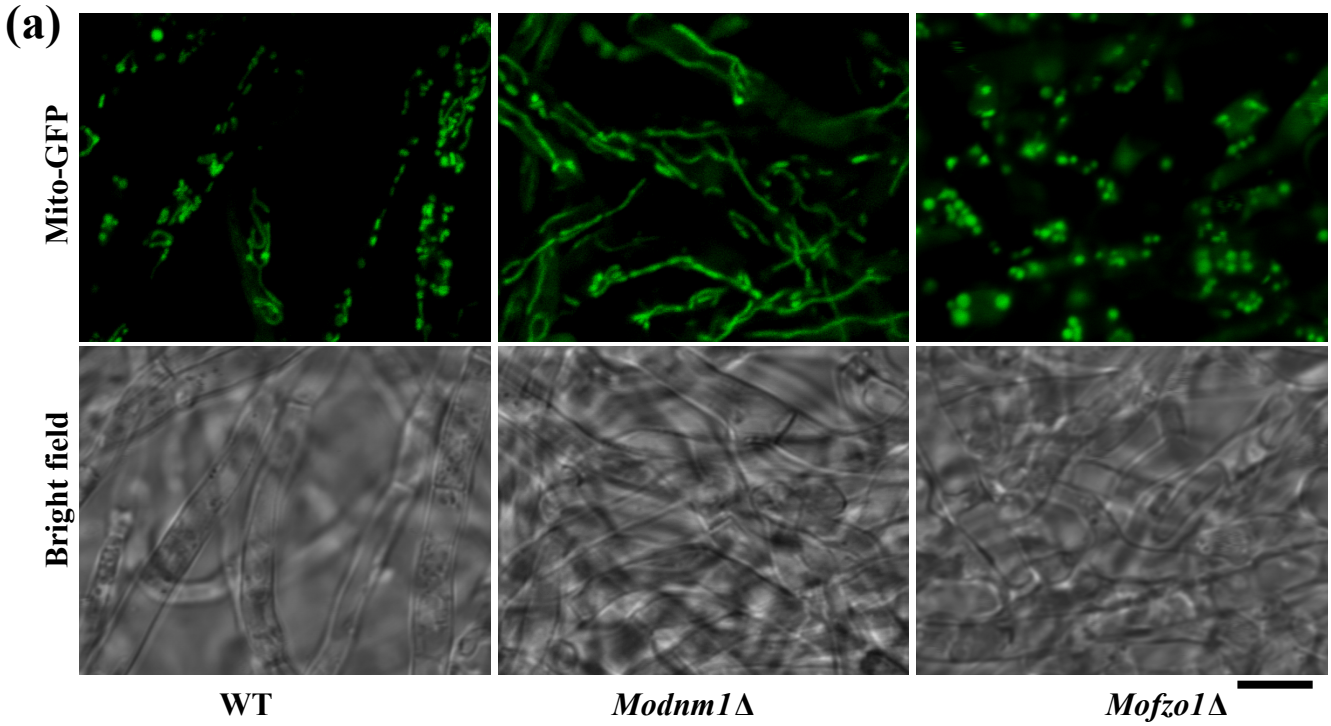

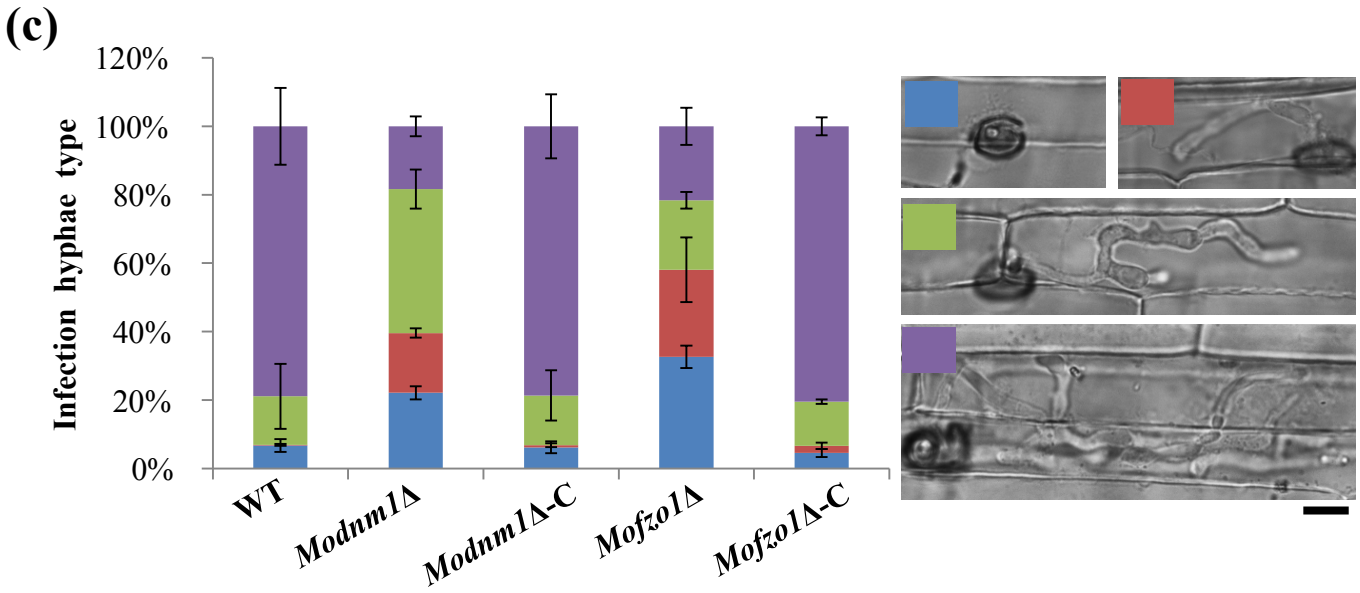

Figure 3

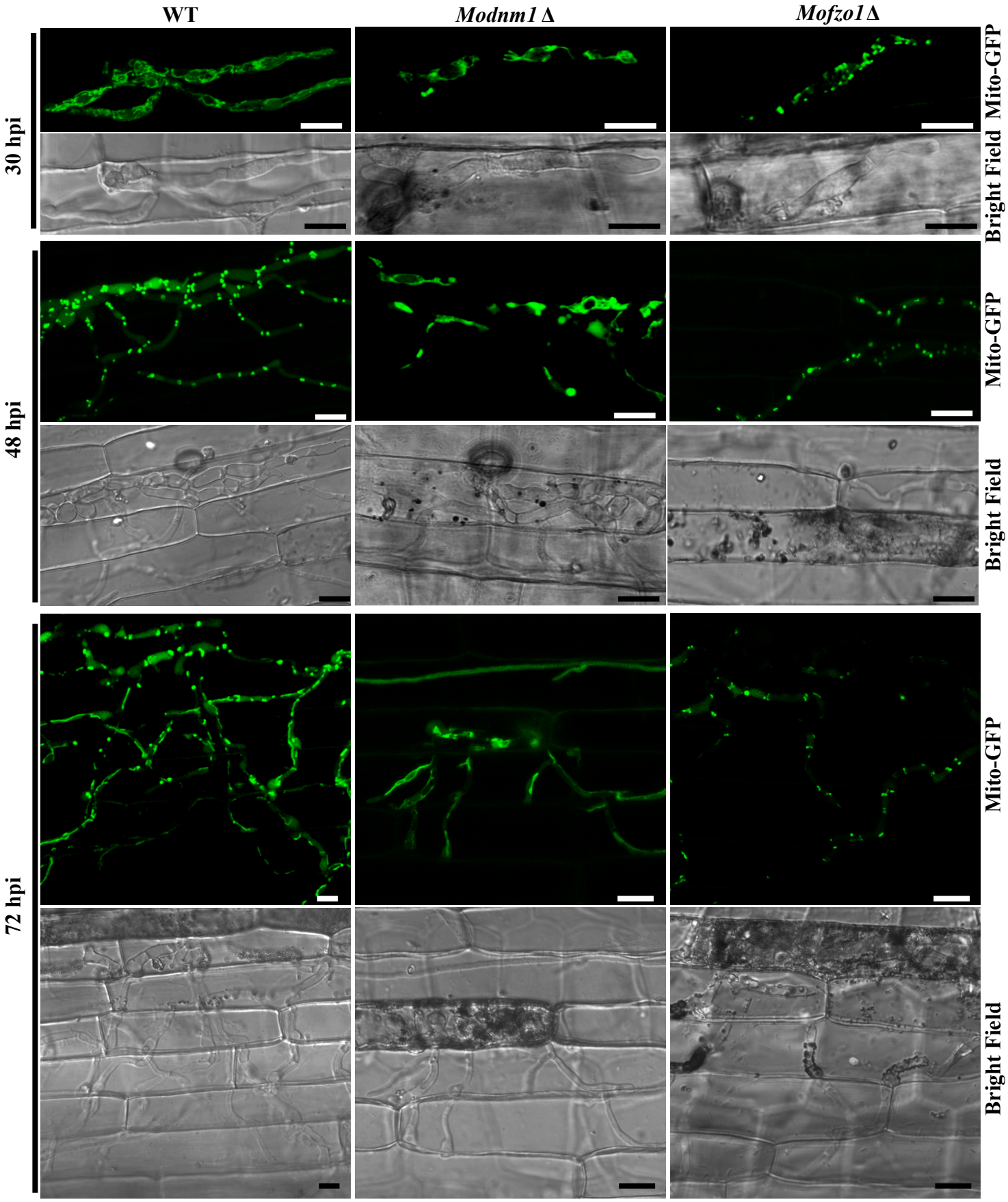

Figure 4

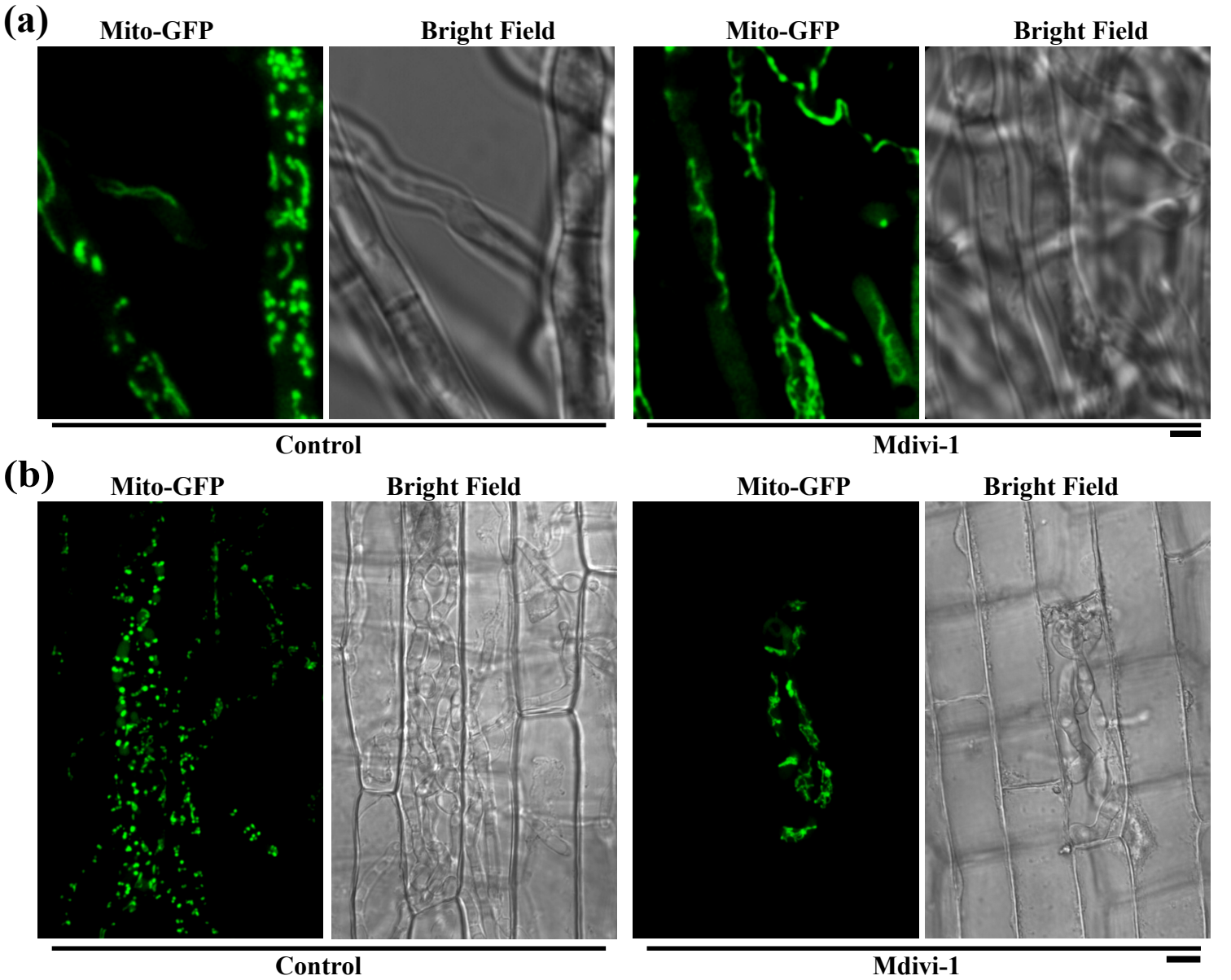

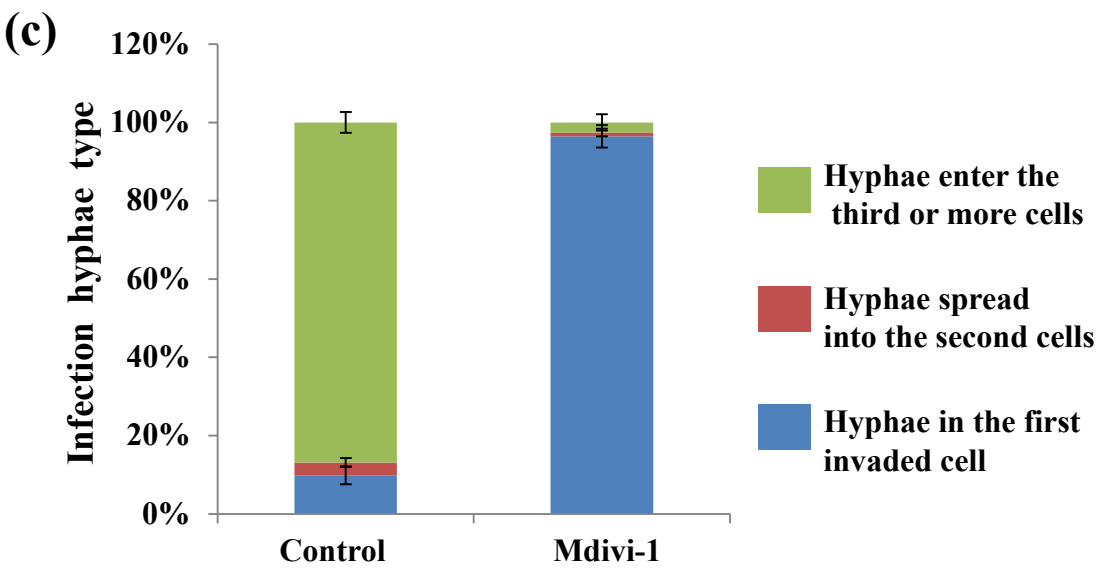

Figure 5

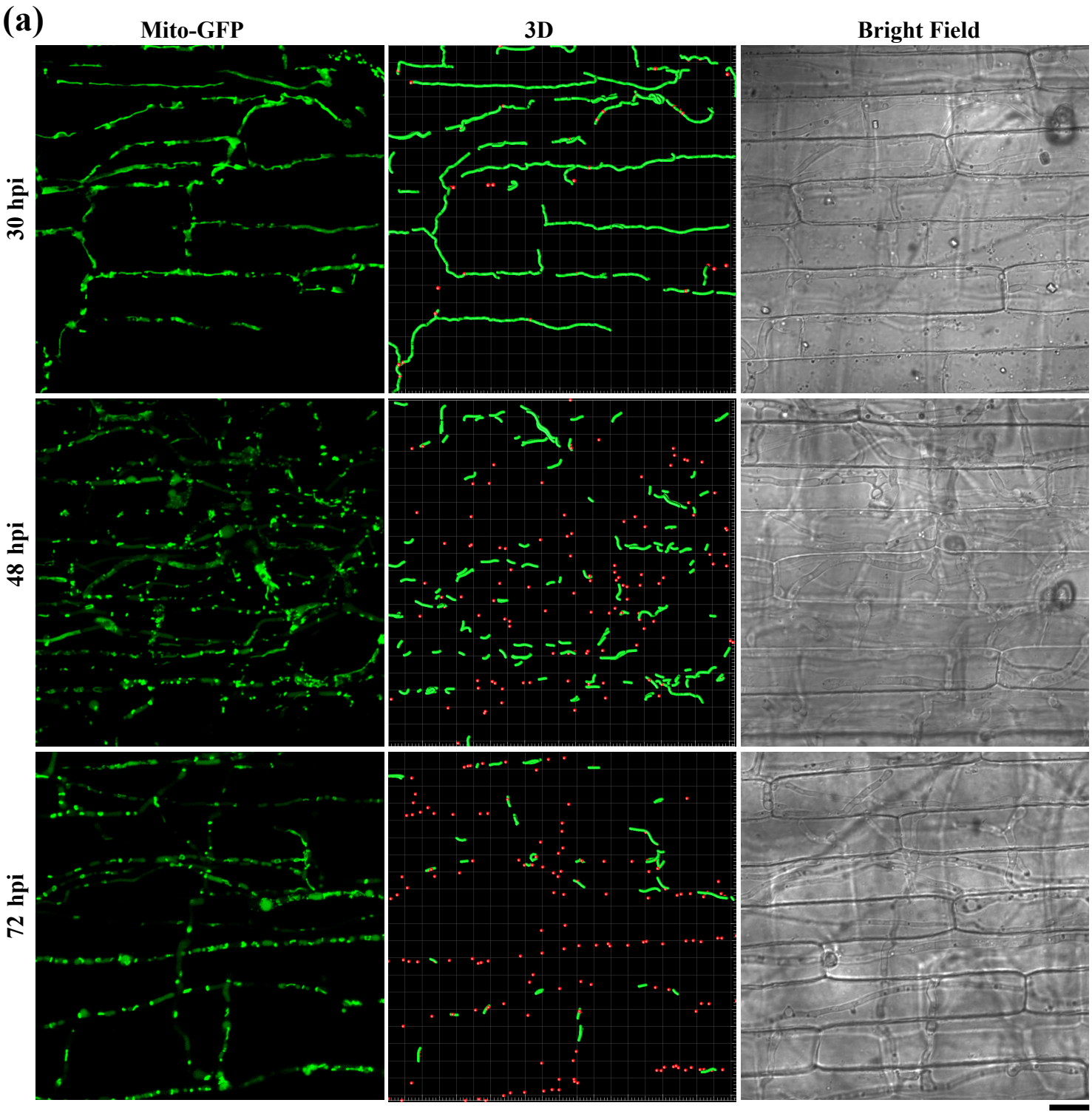

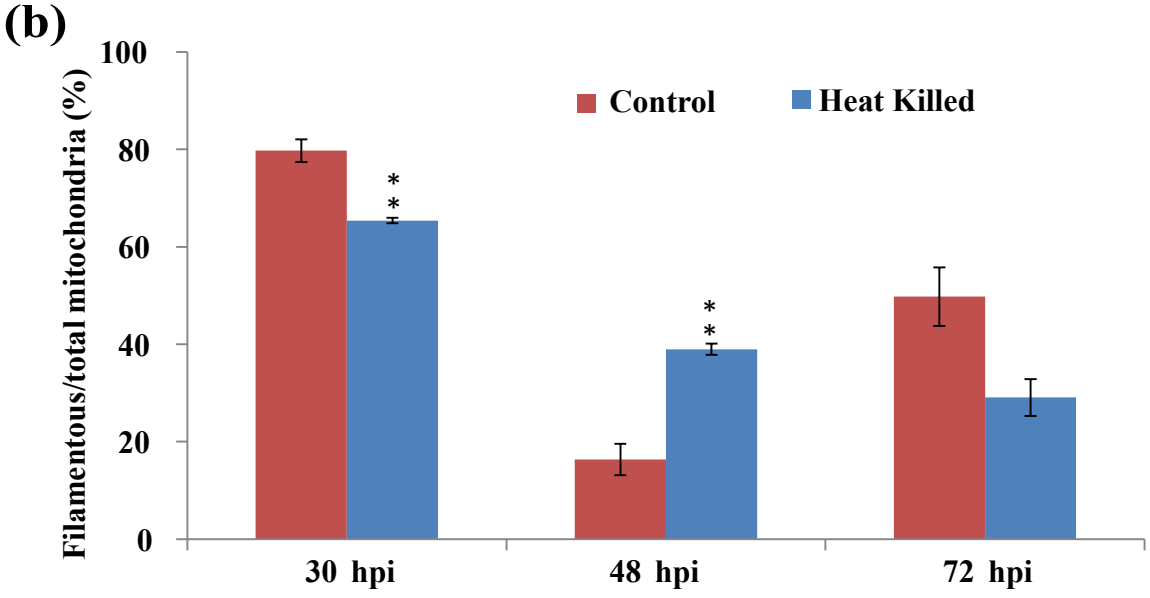

Figure 6

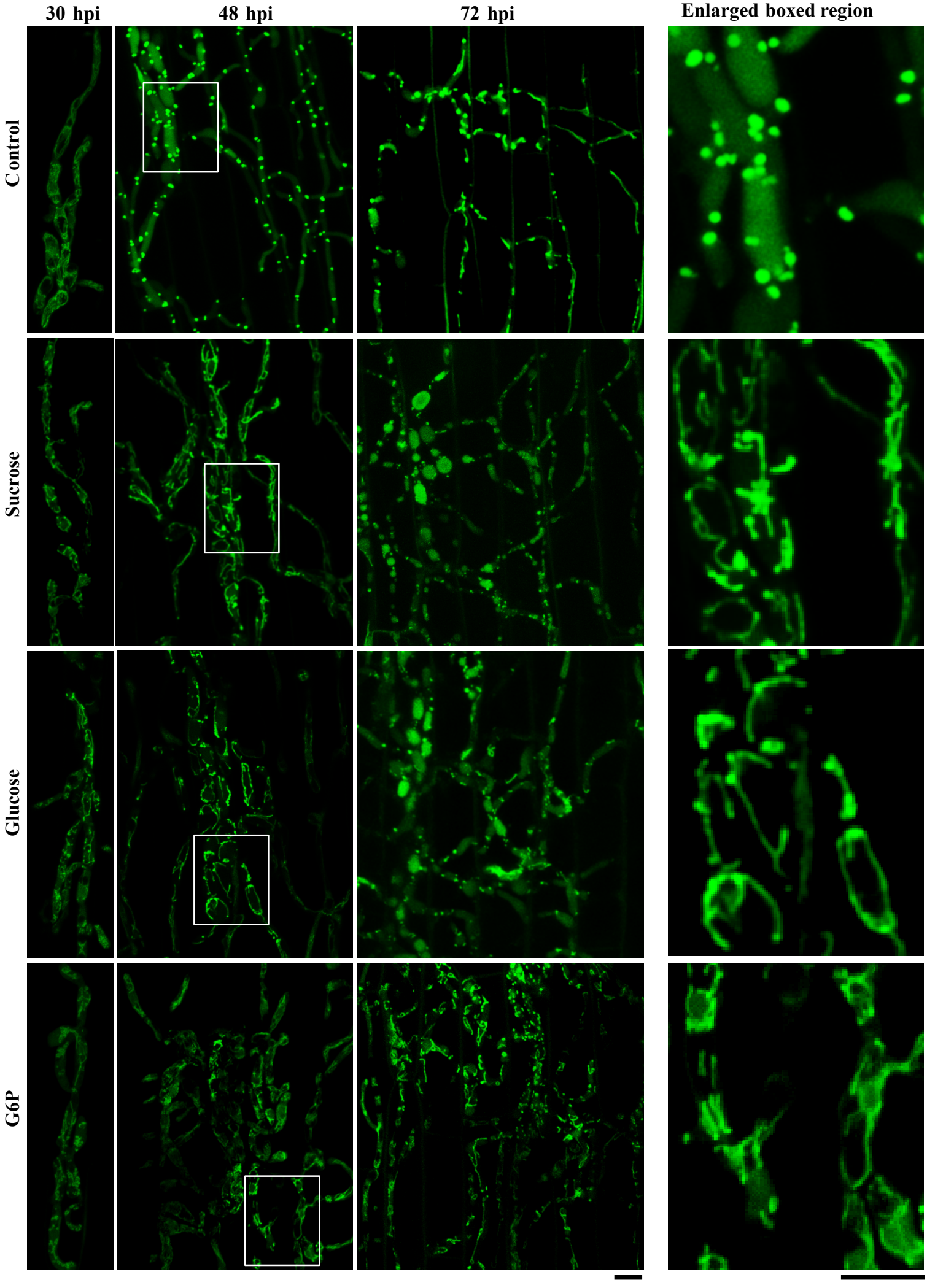

Figure 7

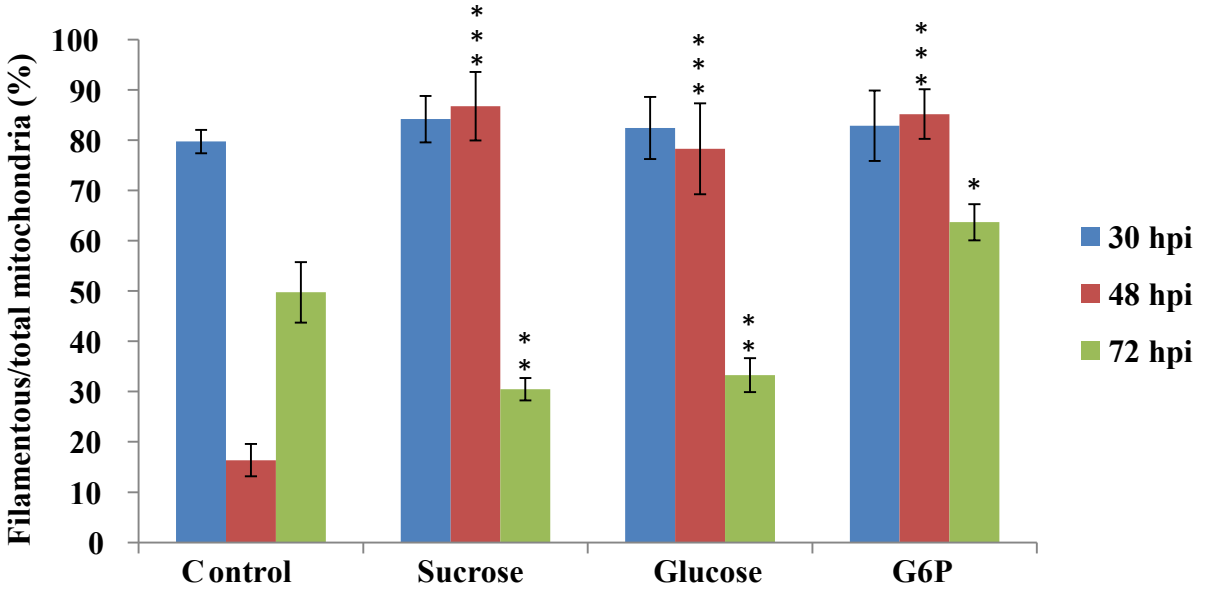

Figure 8